Solar Physics
DOI: 10.1007/•••••-•••-•••-••••-•

Exact solutions for standing kink modes of the longitudinally stratified coronal loops

N. Dadashi[1], H. Safari[2], S. Nasiri[2] and Y. Sobouti[2]

Abstract

The influence of longitudinal structuring on the fast kink modes of coronal loops is investigated. Analytical dispersion relations and mode profiles are derived for the second-order ordinary differential equation governing the z- component of the perturbation in the magnetic field, δB_z. All other components are given in terms of δB_z. Deviations from the frequencies and mode profiles of homogenous loops are given as functions of the density scale height. The effects of the fixed and variable column masses, negative scale heights, and density contrasts inside and outside of the loops are studied. The frequency ratios, mode profiles, and the antinode shifts from those of the sine profiles of the homogenous loops, are tools to estimate solar photospheric parameters. To this end, we have expanded the relevant factors up to the second order in the stratification parameter. In particular, we verify that the first overtone antinode shifts are in the Mm range and are within the reach of the resolutions of the present day observations.

Keywords: Sun, corona; Sun, magnetic fields; Sun, oscillations

1. Introduction

The first spatial oscillations of coronal loops were discovered in extreme ultraviolet (171 $\AA$) by Aschwanden et al. (1999a). Using a MHD wave theory developed by Edwin & Roberts (1983), Aschwanden et al. (1999b) and Nakariakov et al. (1999) interpreted them as the fundamental fast (kink) mode of coronal loops. Subsequently, Wang et al. (2003) observed frequency spectrum of the standing slow modes of the loops.

Since then theoreticians have been supplementing the observed data, oscillation periods, loop lengths, etc., with plausible auxiliary parameters, such as plasma density, magnetic field strength and configuration, etc., with the aim of obtaining reasonably realistic models for the structure of the loops (Bennett et

[1]Zanjan University, Zanjan 45195, Iran,
[2]Institute for Advanced Studies in Basic Sciences, Gava Zang, Po. Box 45195-1159, Zanjan, Iran

al., 1998; Verwichte et al., 2004; Díaz et al., 2002, 2004; Van Doorsselaere et al., 2004; Andries et al., 2005a, b, Arregui et al., 2005; Dymova & Ruderman, 2005; Erdélyi & Fedun, 2006; Díaz & Roberts, 2006; McEwan et al., 2006; Donnelly et al., 2006; Erdélyi & Verth 2007; Dymova & Ruderman, 2005; Dymova & Ruderman, 2006; Verth et al., 2007 Doorsselaere et al., 2007; Erdélyi & Verth, 2007; Safari et al., 2007; Karami & Asvar 2007).

In their recent work, Dymova & Ruderman (2005) and Safari et al. (2007) reduce the MHD wave equations to a single Sturm-Liouville equation for the z-component of the perturbation in the magnetic field. Here, we use the formalism of Safari et al. and show that, for an exponential plasma density stratification along the loop axis, the problem has a closed analytical solution. The loop model, equations of motion, and boundary conditions are presented in Sec. 2. The closed solutions, including the dispersion relation, are treated in Sec 3. Concluding remarks are given in Sec. 4.

2. Description of the model and equations of motion

A coronal loop is approximated by a cylinder of length L and radius R. Loop ends are fixed at the photosphere. Loop curvature is neglected, on account of $R << L$. No initial flow is assumed inside the loop. A uniform magnetic field along the axis pervades the loop, $\mathbf{B} = B\hat{z}$. Gas pressure, gravity and all dissipative and viscous forces are neglected. The density is discontinuous on the lateral surface of the cylinder and varies exponentially along the axis. Thus,

$$\begin{aligned} \rho(r,z,\varepsilon) &= \rho_i(\varepsilon)\exp(-\varepsilon z/L), \quad 0 \le z \le L/2, \text{ inside tube}, \\ &= \rho_e(\varepsilon)\exp(-\varepsilon z/L), \qquad\qquad\quad \text{outside tube}, \end{aligned} \tag{1}$$

where ε is the density scale height parameter, and ρ_i, ρ_e are the interior and exterior footpoint densities, respectively. The assumption of exponential density is in accord with the findings of Aschwanden et al. (1999). They conclude this from their stereoscopic analysis of 30 loop oscillations in EUV. Restriction of z to the interval $[0 - L/2]$ is permissible on account of the symmetry of the loop configuration about its midpoint

The linearized ideal MHD equations are

$$\frac{\partial \rho}{\partial t} + \nabla.(\rho\delta\mathbf{v}) = \mathbf{0}, \qquad \text{Continuity Equation}, \tag{2}$$

$$\frac{\partial \delta\mathbf{v}}{\partial t} = \frac{1}{4\pi\rho}(\nabla \times \delta\mathbf{B}) \times \mathbf{B}, \quad \text{Momentum Equation}, \tag{3}$$

$$\frac{\partial \delta\mathbf{B}}{\partial t} = \nabla \times (\delta\mathbf{v} \times \mathbf{B}), \qquad \text{Induction Equation} \tag{4}$$

$$\nabla.\,\delta\mathbf{B} = \mathbf{0}, \qquad \text{Solenoidal Constraint}, \tag{5}$$

where $\delta\mathbf{v}$ and $\delta\mathbf{B}$ are the Eulerian perturbations in the velocity and magnetic fields, respectively. An exponential φ and t dependence, is assumed, $\exp[-i(m\varphi - \omega t)]$. By straightforward calculations one can express all components of $\delta\mathbf{v}$ and

$\delta\mathbf{B}$ in terms of δB_z. The latter, in turn, is obtained from the following second order PDE (See Safari et al. 2007),

$$\left(\frac{\partial^2}{\partial r^2}+\frac{1}{r}\frac{\partial}{\partial r}+\frac{\partial^2}{\partial z^2}-\frac{m^2}{r^2}+\frac{\omega^2}{v_A^2}\right)\frac{\delta B_z}{B_0}=0, \tag{6}$$

where $v_A(z)=B/\sqrt{4\pi\rho(z)}$, local Alfvén speed, has different values inside and outside of the loop. Equation (6), admits of a separable solution $\delta B_z/B_0 = R(r)Z(z)$, where $R(r)$ satisfies Bessel's equation and will not be further referred to here, and Z satisfies the following

$$\begin{aligned}&\frac{d^2Z(x)}{dx^2}+\Omega^2e^{-\varepsilon x}Z(x)=0, \quad 0\le x=z/L\le 1/2, \qquad (7)\\ &\Omega^2=\frac{L^2\omega^2}{v_{A_i}^2|_{\varepsilon=0}}\frac{\tilde\rho_i(\varepsilon)+\tilde\rho_e(\varepsilon)}{2},\end{aligned}$$

where Ω and $\tilde\rho_{i,e}=\rho_{i,e}(\varepsilon)/\rho_{i,e}(0)$ are dimensionless frequency and footpoint densities, respectively.

Equation (7) is an eigenvalue problem weighted by $\exp(-\varepsilon x)$. Changing the variable x to $\Omega\exp(-\varepsilon x/2)$ reduces Eq.(7) to a Bessel equation with the following solutions

$$Z(x)=c_1J_0(2\frac{\Omega}{\varepsilon}e^{-\varepsilon x/2})+c_2Y_0(2\frac{\Omega}{\varepsilon}e^{-\varepsilon x/2}), \tag{8}$$

where c_1 and c_2 are constants, and J and Y are Bessel functions of first and second kind, respectively. The boundary conditions are

$$\text{for odd modes}\begin{cases}Z(0)=0,\\ Z'(1/2)=0,\end{cases} \tag{9}$$

$$\text{for even modes}\begin{cases}Z(0)=0,\\ Z(1/2)=0.\end{cases} \tag{10}$$

Imposing the boundary condition at $z=0$ on Eq. (8) gives

$$c_1=Y_0(2\frac{\Omega}{\varepsilon}),\quad c_2=-J_0(\frac{2\Omega}{\varepsilon}) \tag{11}$$

Substituting these coefficients in Eq. (8) and imposing the boundary conditions at $x=1/2$ gives the dispersion relations

$$-Y_0(2\frac{\Omega}{\varepsilon})J_1(2\frac{\Omega}{\varepsilon}e^{-\varepsilon/4})+J_0(2\frac{\Omega}{\varepsilon})Y_1(2\frac{\Omega}{\varepsilon}e^{-\varepsilon/4})=0,\quad \text{odd modes}, \tag{12}$$

$$-Y_0(2\frac{\Omega}{\varepsilon})J_0(2\frac{\Omega}{\varepsilon}e^{-\varepsilon/4})+J_0(2\frac{\Omega}{\varepsilon})Y_0(2\frac{\Omega}{\varepsilon}e^{-\varepsilon/4})=0,\quad \text{even modes}. \tag{13}$$

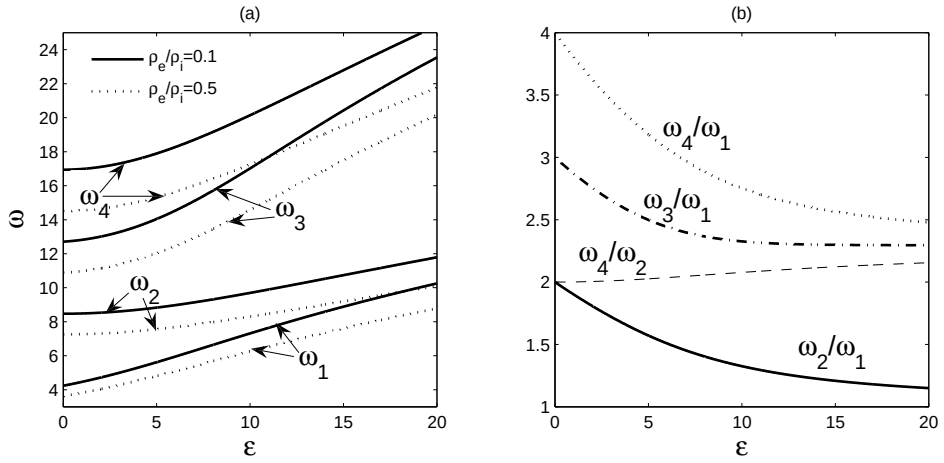

Figure 1. Fundamental and overtone frequencies versus ε. Solid lines for fixed column mass but variable footpoint densities, dashed lines for variable column masses but fixed footpoint density. All frequencies are in units of $\pi v_{A_i}(\epsilon = 0)/L$.

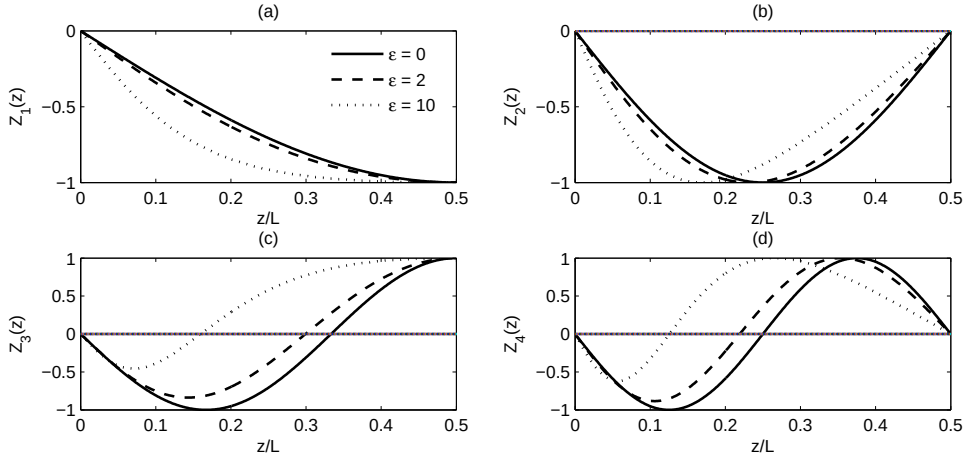

Figure 2. Mode profiles, $Z_n(z)$, *a* ,*b* , *c, d*, corresponding to $n = 1, 2, 3, 4$, respectively. Solid, dashed, and doted lines are for $\varepsilon = 0$, 2, and 10, respectively.

Equations (12) and (13) are similar to those of Díaz & Roberts (2006) with $W \to 0$ in their analysis. In the remainder of this section they are solved analytically for weakly stratified loops and numerically for arbitrary stratifications.

2.0.1. Weak stratification

Bessel functions can be expanded as

$$J_\nu(z) = \sqrt{\frac{2}{\pi z}}\left\{P_\nu(z)\cos z' - Q_\nu(z)\sin z'\right\},\ z' = z - \left(\nu+\frac{1}{2}\right)\frac{\pi}{2},$$
$$Y_\nu(z) = \sqrt{\frac{2}{\pi z}}\left\{P_\nu(z)\sin z' + Q_\nu(z)\cos z'\right\}, \tag{14}$$

where

$$P_\nu(z) \sim 1 - \frac{(4\nu^2-1)(4\nu^2-9)}{128z^2} + O(\frac{1}{z^4}),\quad Q_\nu(z) \sim \frac{(4\nu^2-1)}{8z} + O(\frac{1}{z^3}).$$

We insert Eq. (14) into Eqs. (12) and (13) and reduce them for $\varepsilon \ll 1$ and find

$$\omega_n = \omega_1 \begin{cases} (2n-1)\left(1+\varepsilon(\frac{1}{2^2}+\frac{4}{(2n-1)^2\pi^2}) + \varepsilon^2(\frac{3}{2^7}+\frac{9}{2^2(2n-1)^2\pi^2})\right), & \text{odd,} \\ 2n\left(1+\varepsilon\frac{1}{2^2}+\varepsilon^2(\frac{3}{2^7}-\frac{1}{2^4n^2\pi^2})\right), & \text{even,} \end{cases} \tag{15}$$

where $n = 1, 2, \cdots$, and $\omega_1 = \frac{\pi B}{L}\left[2\pi(\rho_i(0)+\rho_e(0))\right]^{-\frac{1}{2}}$ is the fundamental kink frequency of homogenous loops. Expectedly, $\omega_n \to n\omega_1$ as $\varepsilon \to 0$. The following ratios are noteworthy:

$$\begin{aligned} \tfrac{\omega_2}{2\omega_1} &= 1 - \varepsilon\tfrac{101}{16\pi^2} + \varepsilon^2\left(\tfrac{2525}{64\pi^4}+\tfrac{3535}{2048\pi^2}\right) \\ \tfrac{\omega_{2n-1}}{(2n-1)\omega_1} &= 1 - \varepsilon\tfrac{25}{4\pi^2}\tfrac{(2n-1)^2-1}{(2n-1)^2} + \varepsilon^2\tfrac{125}{2^4\pi^2}(\tfrac{5}{\pi^2}+\tfrac{7}{2^5})\tfrac{(2n-1)^2-1}{(2n-1)^2} \\ \tfrac{\omega_{2n}}{n\omega_2} &= 1 + \varepsilon^2\tfrac{1}{16\pi^2}\tfrac{n^2-1}{n^2} \end{aligned} \tag{16}$$

The frequencies and the ratio of any two odd numbered frequencies begin decreasing linearly with ε. The ratio of two even modes, however, begins decreasing quadratically with ε. These features are also seen on the diagrams of Fig 3*b*. Observational verification of these points, however, has to await the availability of more extended and higher resolutions data. Presently only two frequencies in three loops are available (Verwitche et al. 2004, Van Doorsselaere 2007).

2.0.2. **Arbitrary stratification - Numerical approach**

We use Newton-Raphson's numerical method to solve Eqs. (12) and (13) for the eigenfrequencies. In the range, $0 < \varepsilon = L/H < 20$, the fundamental and three higher kink frequencies, ω_n, $n = 2, 3$, and 4, and the ratios, ω_n/ω_1, are computed. The data are plotted in Fig. 3 for two density contrasts, $\rho_e(\varepsilon)/\rho_i(\varepsilon) = 0.1$ and 0.5. As the density contrast increases the frequencies shift down. Their ratios, however, remain unchanged. The ratio ω_n/ω_1 begins with n and decreases with increasing ε, in compliance with Eqs. (16).

Andries et al. (2005b) maintain that the frequency ratios could be used as a seismological tool to estimate the coronal density scale heights. From the TRACE data, Verwichte et al. (2004) find the ratio ω_2/ω_1 to be 1.64 and 1.81 for loops designated by D and C in their records, respectively. Van Doorsselaere, Nakariakov, & Verwichte (2007) revisited the same ratios from the observational data to be 1.58 and 1.82 for the same loops, respectively, and 1.795 for another loop in their current analysis. With the help of Fig. 1, we find the corresponding ε to be 4.98 and 1.9, respectively. Assuming typical loop lengths, $L = 100 - 400$ Mm, the density scale heights fall in the range of $H = \varepsilon^{-1}L \simeq 20-82$ and $53-210$ Mm, respectively. These scale heights are slightly different from the findings of Andries et al. (2005a,b) and Safari et al. (2007) for a sinusoidal density profile.

A noteworthy point is the effect of column mass on frequencies. In Fig. 1 we assume a constant footpoint density contrast, $\rho_e/\rho_i = 0.1$, and vary ε. Consequently, the total column mass of the loop changes. Compared with variable density contrast but fixed column mass, the mode profiles and the frequency ratios remain unchanged. The frequencies themselves, however, behave slightly differently. For variable column mass models, the frequencies increase more sharply with ε.

The mode profiles, $Z(z)$ of Eq. (8), are shown in Fig. 2 for $n = 1, 2, 3$, and 4. For the unstratified case, $\varepsilon = 0$, the profiles are sinusoidal. With increasing ε, they depart from the sine curves. Antinodes shift toward the footpoints. Stronger the stratification, the greater the shift is, in agreement with the findings of Safari et al. (2007) and Verth et al. (2007). Van Doorsselaere et al. (2007) point out, the shift of the antinodes is potentially, a coronal seismological tool to estimate the density scale heights. In Fig. 3, we have plotted the antinode shift, $z_\varepsilon^{An} - z_{\varepsilon=0}^{An}$, of the first overtone versus ε. The shift $\approx 0.02\varepsilon$, grows approximately linearly with ε. Our numerical result shows that, the shift in the antinode for different density contrasts , $\rho_e/\rho_i = 0.1$ and 0.5, are the same. For typical loops, of lengths $100 - 400$ Mm and density scale heights, $H = 50$ and 100 Mm, the antinode shift falls in the range $2.85 \leq z_\varepsilon^{An} - z_{\varepsilon=0}^{An} \leq 56.64$ Mm and $1.35 \leq z_\varepsilon^{An} - z_{\varepsilon=0}^{An} \leq 25.12$ Mm, respectively. Observation wise, the resolution of current solar satellite facilities, e.g., TRACE, SDO, SO, etc., seems adequate to detect such antinode shifts and estimate the density scale height of solar coronae. Verth et al. (2007) study semi circular loops of sinusoidal density profiles and find the antinode shifts $\approx 0.028\varepsilon$.

Our numerical results show that, for a given ε, the mode profiles are insensitive to changes in density contrast, $\rho_e(\varepsilon)/\rho_i(\varepsilon)$. The differences between the mode profiles of the stratified and unstratified cases, $\Delta Z_n = Z_n(\varepsilon, z) - Z_n(\varepsilon = 0, z)$, $n = 1, 2, 3$, and 4 are plotted in Fig. 4. Erdélyi & Verth (2007) maintains that these differences in the mode profile are so small to be resolved by current EUV instruments of TRACE mission.

Another interesting point is negative scale heights, suggested by Andries (2005a,b) on the basis of the error bars in the observations of Verwichte et al. (2004). Here, the density at the apex is higher than at footpoints. Unlike the positive scale scale height case: a) ω_1 decreases with increasing $|\varepsilon|$, see Fig. 5; b) higher overtones, ω_n, $n = 2, 3, \cdots$, however, increase with $|\varepsilon|$, though at slower

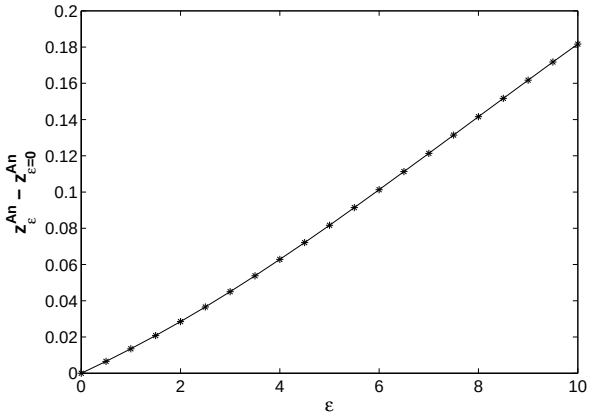

Figure 3. Antinode shift, $z_{\varepsilon}^{An} - z_{\varepsilon=0}^{An}$, (normalized to L) against ε. The shift varies almost linearly with ε

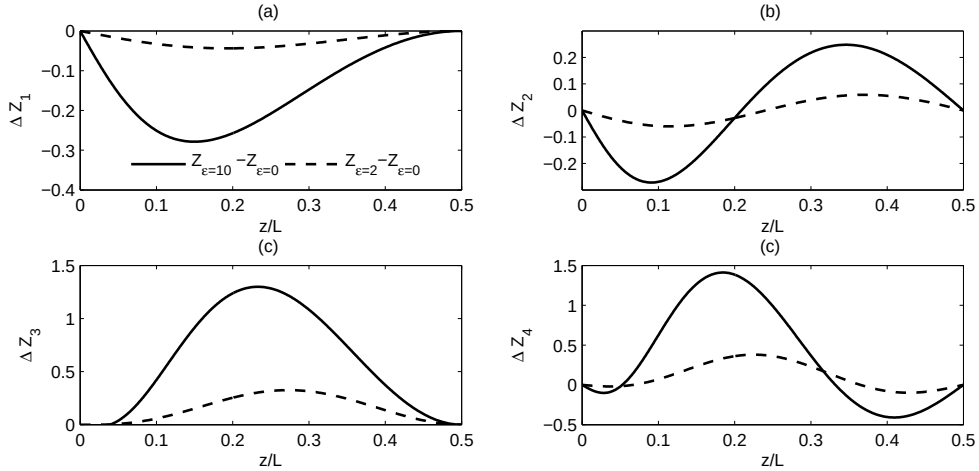

Figure 4. Differences between the eigenprofiles of the stratified and unstratified cases, ΔZ_l, are plotted z.

rate; c) the ratios ω_n/ω_1 increase with $|\varepsilon|$ (not presented in a diagram). As $|\varepsilon|$ increases, the mode profiles and their node and antinodes move away from the footpoints and concentrate more and more in the inner regions of the loop.

3. Conclusions

Suggested theoretical models of 3D coronal loops are, still, far from the realities. Many complicating factors, such as variable cross sections, variable magnetic fields, non-zero β plasmas, etc., are to be accounted for in a realistic study of both the equilibrium structure and the perturbed state of actual loops. Here, we study the oscillations of loops with exponential density variations along the loop axis.

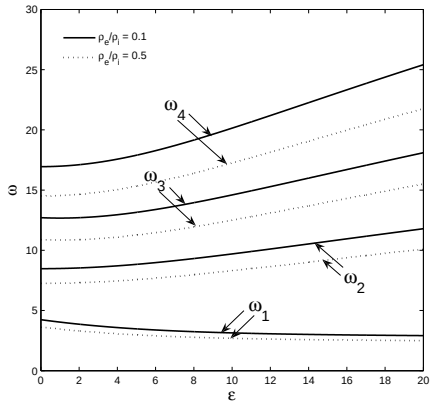

Figure 5. For the case of negative scale heights, the frequencies plotted versus ε, for two different density contrast, $\rho_e/\rho_i = 0.1$ (solid lines) and $\rho_e/\rho_i = 0.5$ (dotted lines).

- Analytical dispersion relations, Eqs. (12) and (13), and analytical mode profiles, Eq. (8) and Fig. 2, are derived.

- For weak stratifications, the kink frequencies and the frequency ratios are found up to the second order in ε, Eqs. (15) and (16).

- Increasing the density contrast decreases the frequencies but their ratios and shape of the profiles remain unchanged.

- Models with variable total column mass, but constant footpoint densities, are investigated. Compared with models of constant total mass, the frequencies increase more sharply with increasing ε.

- The case of negative scale heights is investigated and results are compared with those of positive ε's.

- For $1.58 \leq \omega_2/\omega_1 \leq 1.82$, and for typical loop lengths, 100-400 Mm, the density scale heights fall in the range of 20-210 Mm, in agreement with Andries et al. (2005a, b), Safari et al. (2007), McEwan et al. (2006), and Donnelly et al. (2006).

- Based on our simple theoretical model and typical coronal conditions, the antinode shift of the first overtone mode profiles are in the range of $1.3-56.6$ Mm. They are in the range of the detectability of the resolution of the current observational instruments.

References

Andries, J.; Goossens, M.; Hollweg, J. V.; Arregui, I.; & VanDoorsselaere, T.: 2005a, *Astron. Astrophys.*, **430**, 1109.
Andries, J.; Arregui, I.; & Goossens, M.: 2005b, **624**, 57.

Aschwanden, M. J.; Fletcher, L.; Schrijver, C. J.; & Alexander, D.: 1999a, *Astrophys. J.*, **520**, 880.
Aschwanden, M. J.; Newmark, J. S.; *et al.*: 1999b, *Astrophys. J.*, **515**, 842.
Bennett, K.; Roberts, B.; & Narain, U.: 1999, *Solar Phys.*, **185**, 41.
Díaz, A. J.; Oliver, R.; & Ballester, J. L.: 2002, *Astrophys. J.*, **580**, 550.
Díaz, A. J.; Oliver, R.; Ballester, J. L.; & Roberts, B.: 2004, *Astron. Astrophys.*, **424**, 1055.
Díaz, A. J. & Roberts, B.: 2006, *Astron. Astrophys.*, **458**, 975.
Donnelly, G. R.; Díaz, A. J.; & Roberts, B.: 2006, *Astron. Astrophys.*, **457**, 707.
Dymova, M. V. & Ruderman, M. S.: 2005, *Solar Phys.*, **229**, 79.
Dymova, M. V. & Ruderman, M. S.: 2006, *Astron. Astrophys.*, **459**, 241.
Edwin, P. M. & Roberts, B.: 1983, *Solar Phys.*, **88**, 179.
Erdélyi, R. & Fedun, V.: 2006, *Solar Phys.*, **238**, 41.
Erdélyi, R. & Verth, G.: 2007, *Astron. Astrophys.*, **462**, 743.
Karami, K.; Nasiri, S.; & Sobouti, Y.: 2002, *Astron. Astrophys.*, **396**, 993.
Karami, K. & Asvar, A.: 2007, *MNRAS*, **381**, 97.
Nakariakov, V. M.,; Ofman, L.; DeLuca, E.; Roberts, B.; & Davila, J. M.: 1999, *Science*, **285**, 862.
McEwan, M. P.; Donnelly, G. R.; Díaz, A. J.; & Roberts, B.: 2006, *Astron. Astrophys.*, **460**, 893.
Safari. H.; Nasiri. S.; Karami, K.; & Sobouti, Y.: 2006, *Astron. Astrophys.*, **448**, 375.
Safari, H.; Nasiri, S.; & Sobouti, Y.: 2007, *Astron. Astrophys.*, **465**, 1111.
Van Doorsselaere, T. V.; Andries, J.; Poedts, S.; & Goossens, M.: 2004, *Astron. Astrophys.*, **606**, 1223.
Van Doorsselaere, T.; Nakariakov, V. M.; & Verwichte, E.: 2007, *Astron. Astrophys.*, **473**, 959.
Verth, G.; Van Doorsselaere, T.; Erdélyi, R., & Goossens, M.: 2007, *Astron. Astrophys.*, **475**, 341.
Verwichte, E.; Nakariakov, V. M.; Ofman, L.; & Deluca, E. E.: 2004, *Solar Phys.*, **223**, 77
Wang, T. J.; Solanki, S. K.; Innes, D. E.; Curdt, W.; & Marsch, E.: 2003, *Astron. Astrophys.*, **402**, L17.